Analysis of a Static Loading Test on an Instrumented Cased CFA Pile in Silt and Sand

Jakub G. Kania, *Industrial Ph.D. Student, cp test a/s / Aarhus University, Vejle/Aarhus, Denmark; email: jakub@cptest.dk*
Kenny Kataoka Sørensen, *Associate Professor, Department of Engineering, Aarhus University, Aarhus, Denmark; email: kks@eng.au.dk*
Bengt H. Fellenius, *Consulting Engineer, Sidney, BC, Canada, V8L 2B9; email: bengt@fellenius.net*

ABSTRACT: *A static loading test was performed on an instrumented 630 mm diameter, 12.5 m long, cased continuous flight auger (CFA) pile. The soil at the site consisted of a 4.0 m thick layer of loose sandy and silty fill layer underlain by a 1.6 m thick layer of dense silty sand and sand followed by dense sand to depth below the pile toe level. The instrumentation comprised vibrating wire strain gages at 1.0, 5.8, 9.4, and 12.0 m depth. The pile stiffness (EA) was determined by the secant and tangent methods and used in back-calculating the distributions of axial load in the pile. A t-z/q-z simulation of the test was fitted to the load-movement distributions of the pile head, gage levels, and pile toe. The load-movement response for the shaft resistance was strain-hardening. The records indicated presence of residual force. Correction for the residual force gave a more reasonable shaft resistance distribution and indicated an about 600 kN residual toe force.*

KEYWORDS: Soil-pile interaction, load-transfer functions, beta-coefficient, residual force, vibrating wire strain gage

SITE LOCATION: Geo-Database

INTRODUCTION

This paper presents results from a static loading test on an instrumented cased CFA pile embedded in silt and sand. The pile type is somewhat new to the Danish practice which mostly uses driven precast concrete piles. Only limited local experience is available on bored piles, notably, cased CFA piles. However, the bored pile is widely used internationally (e.g., Touma and Reese 1972, Gwizdała 1984), and Platzek and Gerressen (2010) describe the cased CFA pile.

In regard to piled foundations, the Danish practice is regulated and mandated by the National Annex to the Eurocode (DS/EN 1997-1 DK NA:2015), which limits the shaft resistance of bored piles to 30% of that for a similar driven pile and the unit toe resistance of bored piles to 1,000 kPa, unless a larger bearing resistance can be demonstrated. This principle was introduced in the Danish code for foundations in 1977 with some adjustments in 1984 and 1998 (Knudsen et al. 2019). The restriction limits the use of bored piles in Denmark.

The paper presents a case study of the response of cased CFA piles in silt and sand. The results support modifying the rules regarding bored piles constructed as cased CFA piles in the National Annex to the Eurocode.

MATERIALS AND METHODS

Soil Profile

The construction site was located in Viborg, Denmark. Prior to the pile test, the site was excavated to between 2 to 3 m depth over a 50 by 120 m area. The test pile was installed at 3 m distance from the nearest excavation, sloping 1(H)-1.5(H):1(V). Figure 1 shows the results of a CPT sounding pushed 8 m from the test pile. Figure 2 shows the CPT soil classification chart according to the Eslami-Fellenius method (Eslami 1996). The classification is also indicated at the right of Figure 1.

Submitted: 15 December 2019; Published: 18 November 2020
Reference: Kania J. G., Sørensen K. K., and Fellenius B. H., (2020). Analysis of a Static Loading Test on an Instrumented Cased CFA Pile in Silt and Sand, International Journal of Geoengineering Case Histories, Vol.5, Issue 3, p. 170 - 181. doi: 10.4417/IJGCH-05-03-03

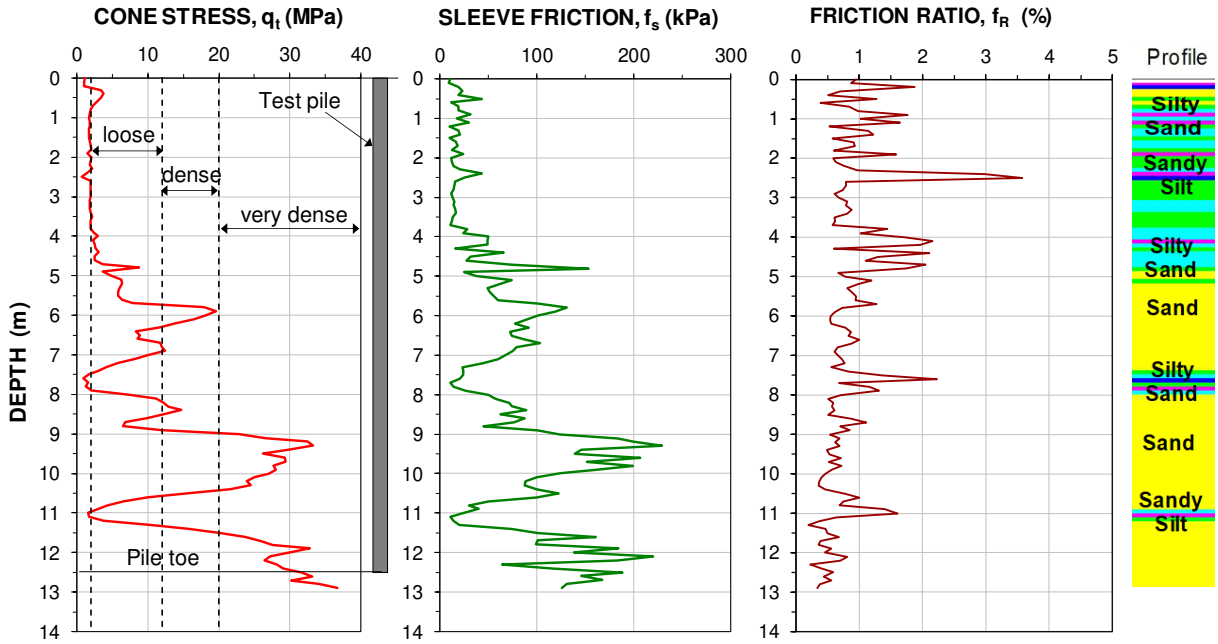

Figure 1. Results of a CPT sounding pushed 8 m from the test pile.

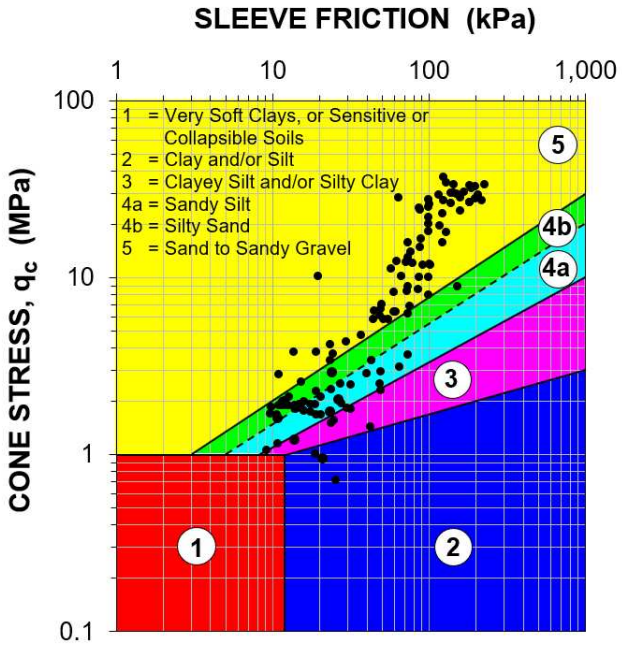

Figure 2. CPTU soil classification chart according to the Eslami-Fellenius method (Eslami 1996).

The soil profile below the excavation level consists of three layers, as follows:

- Sandy and silty fill to about 4.0 m.
- Silty sand and sand to 5.6 m.
- Sand to the end of the CPTU sounding at 13 m depth with a zone of silty sand and sandy silt.

The sand between 5.6 and 9 m depth is loose, except for a 0.8 m thick dense zone at 6 m depth and a very loose zone of silty sand at about 7.7 m depth. Below 9 m depth, the sand is dense to very dense, except for an about 0.3 m thick zone of loose sandy silt at 11 m depth.

Figure 3a shows the soil profile and water content distribution (the distances to the test pile location are indicated in the figure caption). The water content was determined on relatively intact samples considered to have neither gained nor lost water due to the sampling process. The average water content to 5.4 m depth was about 14%. The water content of the sand layer was about 3% at 5.7 m depth increasing to about 15% at 12.7 m depth with an intermediate 25% silty layer at 8.7 m depth. The groundwater table was at about 9.7 m depth (measured June 30, 2016). The unit densities, according to the geotechnical report (GEO 2016), were on average 1,900, 1,700, and 1,800 kg/m^3 of the fill, silty sand, and sand, respectively. Figure 3b shows the undrained shear strength obtained from field vane test and calculated from CPT profile using N_k equal to 15, as conventionally recommended. The shear strength, c_u, of the fill layer obtained from the field vane test is similar to the distribution of the vertical effective stress. The shear strength obtained from the CPT ($c_u = q_t/N_k$ with N_k=15) is about three times greater than the one obtained from the field vane test.

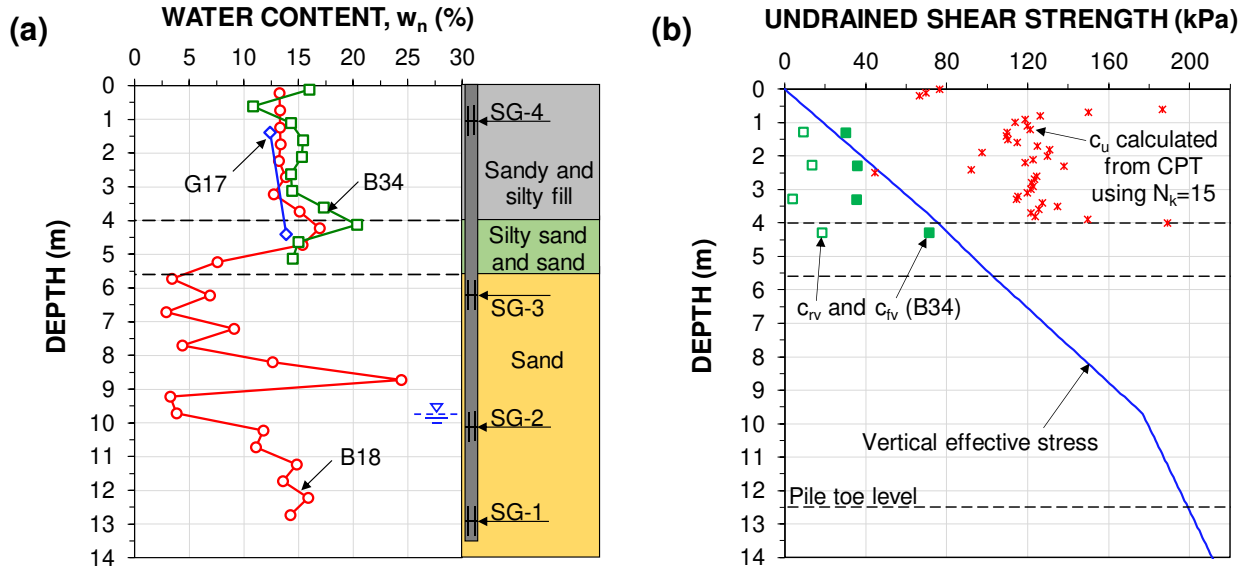

Figure 3. (a) Soil profile and distribution of water content. Data are from three soil borings: B34 (performed in October, 1989; 13 m from the test pile), B18 (performed in December, 2014; 27 m from the test pile), and G17 (performed in June, 2016; 8 m from the test pile); (b) undrained shear strength determined from the field vane test (peak, c_{fv}, and remolded, c_{rv}), CPT, and the distribution of vertical effective stress.

Test Pile

The test pile was a nominal 630 mm diameter, cased CFA pile drilled to a depth of 12.5 m on July 13, 2017. After augering to the final depth, the concrete was pumped through the hollow stem of the auger, while withdrawing the auger with the casing. When the casing end was withdrawn to about 7 m depth, the supply of concrete was unintentionally suspended, halting the concreting process. Within less than 3 hours after the interuption of the initial concreting process, the pile was re-augered to the original depth (i.e., 12.5 m). The concreting process was then restarted and successfully finished. The pile head was encased with a 630-mm diameter, 1,000 mm long pipe that was accidentally placed 30 mm off center with the reinforcing cage. The pile stick-up (height above the ground surface) was 300 mm.

Vibrating wire (VW) sister-bar strain gages (SG) were installed at four depths (one opposite mounted pair at each level): 12.0 m (SG-1), 9.4 m (SG-2), 5.8 m (SG-3), and 1.0 m (SG 4). The gages were mounted on a 470 mm diameter reinforcement cage placed centrically in the pile. Thus, the nominal thickness of the concrete cover was 80 mm. The cage consisted of twelve 20 mm diameter main reinforcing bars and 12 mm spiral reinforcement on 150 mm spacing. Additionally, the reinforcing cage had 6x60 mm flat bar stabilizing rings spaced every 970 mm. The 1 m long lowermost section of the cage was tapered to 320 mm diameter and consisted of six 20 mm diameter, 1.8 m long reinforcing bars (0.8 m overlap).

The test setup is presented in Figure 4. Before constructing the test pile, two groups of four piles of reaction piles were installed to 12.5 m depth. The free distance between the test pile and the closest reaction pile was 2.9 m (4.6 pile diameters). Each reaction pile was connected via a Dywidag bar to a system of reaction beams. A steel reference frame was anchored about 2.5 m from the test pile and the nearest reaction piles, covered by a tarp to protect it from sunlight. Details about the test setup are reported in Kania and Sørensen (2018). No telltales were installed.

Figure 4. The test setup.

Test Procedure

A static pile loading test was carried on July 27, 2017, on the 14th day after the concreting of the test pile. The pile load was applied by a single hydraulic jack centered to the steel-pipe encased pile head and operated by an automatic load-holding pump. The load applied to the pile was measured with a load cell connected to a data logger. The pile-head movement was monitored with three inductive displacement transducers also connected to the data logger.

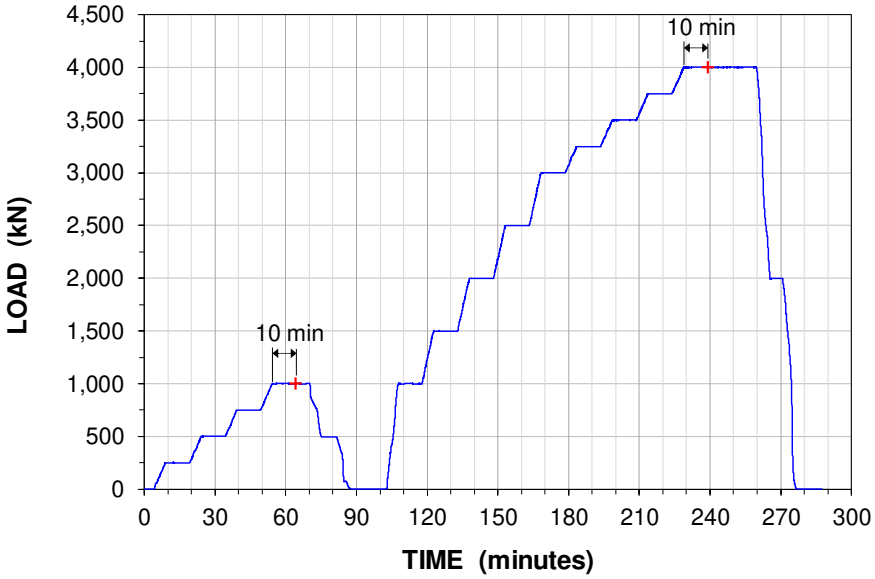

Figure 5. Load-time schedule (Data from Aamann-Svale and Møller 2017).

All gages and sensors were recorded at 1-second intervals. The test schedule is presented in Figure 5. The loading schedule comprised two loading stages. During the first stage, the load was increased to 1,000 kN in four 250 kN increments. Adding each increment took about 5 minutes and, afterward, the load levels were maintained for about 10 minutes. The 1,000 kN maximum load was maintained for 15 minutes, whereupon the pile was unloaded in two 500kN steps with the half-load value maintained for 5 minutes. After a 15-minute wait, the pile was re-loaded to 1,000 kN in one step. Then, 500 kN load increments were applied to a total load of 3,000 kN. Beyond 3,000 kN load, the load increments were 250 kN. The final load was 4,000 kN. After 30 minutes of load-holding, the pile was unloaded in two 2,000 kN load steps. Each unloading step took 5 minutes and the half-load was maintained for 5 minutes.

TEST RESULTS

Pile-head Load-movement Curve

Figure 6a shows the pile-head load-movement records and demonstrates that the load-holding device functioned well. At the 4,000 kN maximum load, the movement for the 5 minutes of adding load and the following 10-minute load holding resulted in a 2.1 mm pile-head movement. The movement over the subsequent 20-minute extended load holding was only 0.4 mm. The maximum pile-head movement amounted to 16 mm. Figure 6a shows that after reaching each intended load level, only small additional movement was recorded. The average movement rate for the last 5 minutes at any load level ranged from zero to 0.05 mm/min. The fast stabilization of movement is typical for piles in cohesionless soils.

Strain Measurements

Figure 6b shows the strains measured at each gage of the four gage-level pairs. The uppermost gage pair (SG-4A and SG-4B at 1.0 m depth) showed that bending occurred at the gage level, presumably due to the mentioned off-center placement of the short steel pipe at the ground surface. Bending was less pronounced for the other three gage levels. The axial force in the pile was determined from the average of the strain-gage pair at each gage level and the bending did not affect the evaluated axial loads.

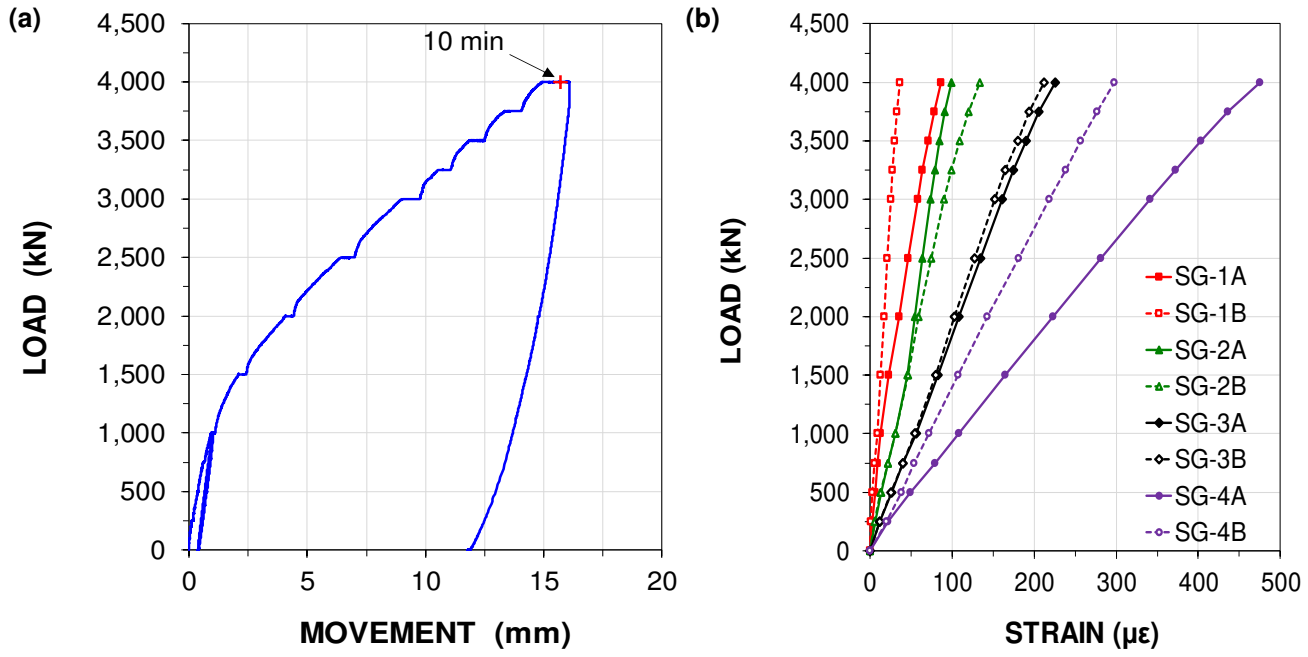

Figure 6. (a) Load-movement records of the test (Data from Aamann-Svale and Møller 2017); (b) strains measured at last reading for each gage level.

ANALYSIS

Pile Stiffness

Figure 7 shows the measured load-strain records (average between two opposite strain gages) for Gage Levels SG-1 through SG-4. Generally, for gage levels at depths where the pile section between the gage level and the pile head is affected by a perfectly plastic-response shaft resistance, the load-strain lines first rise steeply and become parallel when the resistance along the length above the strain gage location has been fully mobilized (Fellenius 2020). The slope of the straight portion of the lines then represents an approximate value of the pile stiffness. However, although the lines from the subject test results are straight, none of the lines indicate a change that would suggest full mobilization of shaft resistance and the lines are not parallel. This is an indication that the soil at the imposed movement has not developed a perfectly plastic response, but instead the soil response continues to be strain-hardening. Moreover, the linear regression of the line for SG-4, the gage level that was essentially unaffected by shaft resistance, does not extend to the origin, but shows an approximately 50 kN initial force in the pile. This could be due to the combined effect of the bending induced by the off-center placement of the jack in relation to the reinforcing cage at the pile head. As a result, the gage pair average may not correspond to the pile center. The stiffness difference between the pile portion encased by the steel pipe and the portion without the steel pipe would then occur 300 mm above SG-4. The unloading-reloading and/or a small contribution of shaft resistance along the 1,000 mm length from ground surface to SG-4 also contribute. The conditions combine to make the analysis of the pile axial stiffness by the direct secant modulus less precise.

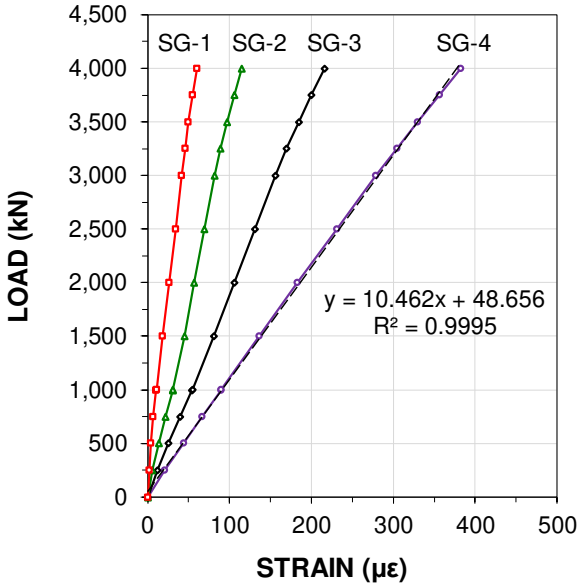

Figure 7. Load-strain from strain-gage levels SG-1 to SG-4 (last reading at each load-level).

The E-modulus of a concrete pile is often not a constant over the range of the applied loads, but diminishes for increasing load (stress). Moreover, for cast-in-situ piles, the pile cross sectional area can differ from the nominal area along the pile. However, the pile axial stiffness, EA/L (the length, L, is usually set to 1 m), at a gage level usually shows a linear relation to the imposed strain. The stiffness can be determined directly from the test records (Fellenius 1989). The procedure provides a relation between the line showing tangent stiffness, E_tA, and the line showing secant stiffness, E_sA, as functions of the slope, a, and ordinate intercept, b, where $E_tA = \varepsilon a + b$ and $E_sA = 0.5\varepsilon a + b$. The tangent-modulus method does not depend on accurately knowing the zero reference of the strain records, but it does depend on having consistently well-established records unaffected by occasionally prolonged load-holding and unloading and reloading events. In contrast, the direct secant-modulus method is strongly affected by an error in the zero reference of the strain records as well as any prolonged load-holding and unloading and reloading events (Fellenius 2012; 2020).

Figure 8a shows the tangent modulus stiffness line for the subject test. The solid line with filled symbols shows the records for the reloading of the pile. The open-symbol line shows the records for the virgin loading. For the records from SG-4, where essentially no shaft resistance occurs, a relation for the tangent stiffness, E_tA, line could be determined. However, for the

gage levels down in the soil, no linear tendency was established. Yet, the maximum movement between the pile relative to the soil was 16 mm, significantly larger than 5 mm, a movement at which it is usually considered that the shaft resistance is fully mobilized (Fellenius 2020). For example, Nguyen and Fellenius (2013) reported a case with full mobilization of shaft resistance along 1,800 mm diameter, bored piles occurring at movements of 3 to 5 mm.

Possibly, the tangent modulus line for SG-3 could have developed a straight-line tendency if the test had continued beyond the 16 mm maximum movement. However, that line would then have been located significantly above the line for SG-4. Indeed, the non-equal location of the lines and the potential late establishment of the tangent modulus lines is a further indication that the soil at the site is strain-hardening (Fellenius and Nguyen 2019).

Figure 8b shows the secant stiffness (E_sA) versus strain records from SG-4, the gage level 1.0 m below the pile head. The purple solid line with filled symbols shows the secant stiffness for the reloading of the pile. The purple solid line with open symbols presents the records for the virgin loading. The blue straight line indicates the secant stiffness relation for the reloading of the pile. The green straight-line without symbols shows the secant line converted from the tangent modulus method.

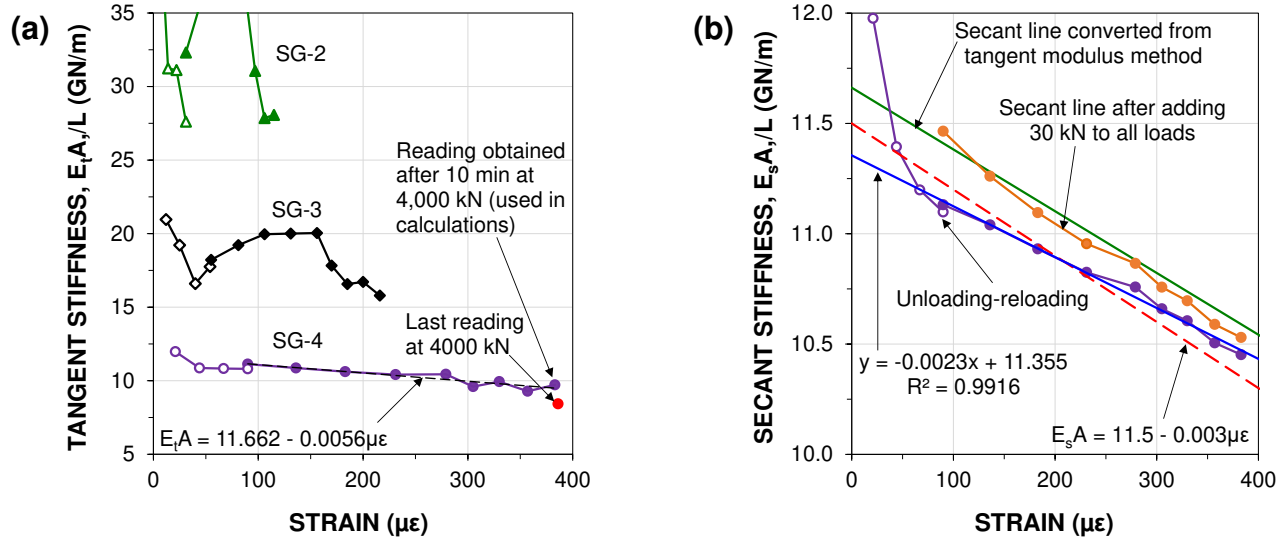

Figure 8. (a) Tangent and (b) secant stiffness versus strain from SG-4. Pile stiffness determined for one meter unit length.

A direct secant line may be affected by several undesirable effects, such as presence of a shaft resistance, incorrect reference to "zero-strain" (i.e., residual strain at the gage level), incorrect load values (e.g., using the pump pressure to obtain the applied load instead of an accurate load cell), differing length of load holding, and any unloading-reloading event. Normally, the secant lines determined by the direct secant and tangent methods agree (with due allowance to the larger scatter of the tangent method caused by the data differentiation). However, this is not the case here. As shown, when simulating uncertainty in the zero reference by adding a 30 kN load to each measured load value, the secant method line (orange solid line with filled symbols) moves in close proximity to the secant line converted from the tangent modulus method. The probable cause of the difference is the unloading-reloading event, although influence due to the proximity of SG-4 to the pile head (2 pile diameters) and the off-center load application cannot be ruled out. In the subsequent analysis it was decided to apply the following secant line relation (indicated by the dashed red line in the figure):

$$E_sA\ (GN) = 11.5 - 0.003\mu\varepsilon \quad (1)$$

Measured and Simulated Load Distributions

Figure 9 shows the load distributions for all loads applied in the reloading phase as converted from the measured strains using the secant stiffness. The two intermediate half-size loads employed in the test are shown as dashed lines. The 3,000 kN load that generated a 9.8 mm pile-head movement was chosen as the Target Load for the analysis. The red line shows the Target Load distribution.

A fit to the measured distribution of forces was first obtained by back-calculating the axial forces at Gage-Levels SG-1 through SG-4 for the 3,000 kN Target Load. The distribution of unit shaft resistance corresponding to the Target Force distribution was then correlated to the distribution of effective stress, which gave the distribution of the correlation coefficient, conventionally termed "beta (ß)-coefficient". The $ß_{trg}$-coefficients that gave the fit for the shaft resistance in-between the gage levels are listed in the table to the right of the graph. The list also includes the corresponding average unit shaft resistances, r_s (kPa), for in-between the gage levels. It should be realized that the $ß_{trg}$-coefficients represent the ratios between the back-calculated unit shaft resistance and the effective overburden stress as mobilized at the Target Movement, and are not intended to indicate ultimate resistance.

The simulation assumed a level ground surface around the test pile. However, the area around the test pile was not fully level and the excavation slope was only about 3 m away from the test pile. Therefore, the effective overburden stress would have been somewhat larger than assumed in the simulation. A repeat analysis including the increase of the effective stress, along the test pile due to load imposed by the area outside the project calculated for a wide embankment sloping 1(H)-1.5(H):1(V) upward from a point 3.0 m away from the test pile, showed that this would reduce the $ß_{trg}$ -coefficients in the lower layers from 0.43 to 0.41; i.e., by 5% in the lower part of the pile and a difference of about 100 kN (1%) in total resistance. However, showing results to more than one decimal precision would essentially be just for "cosmetic" reason; the about 2 m elevation difference is too small to have had any significant effect on the test pile response to the applied load. The calculations applied Boussinesq distribution and were performed using the UniPile5 software (Goudreault and Fellenius 2014).

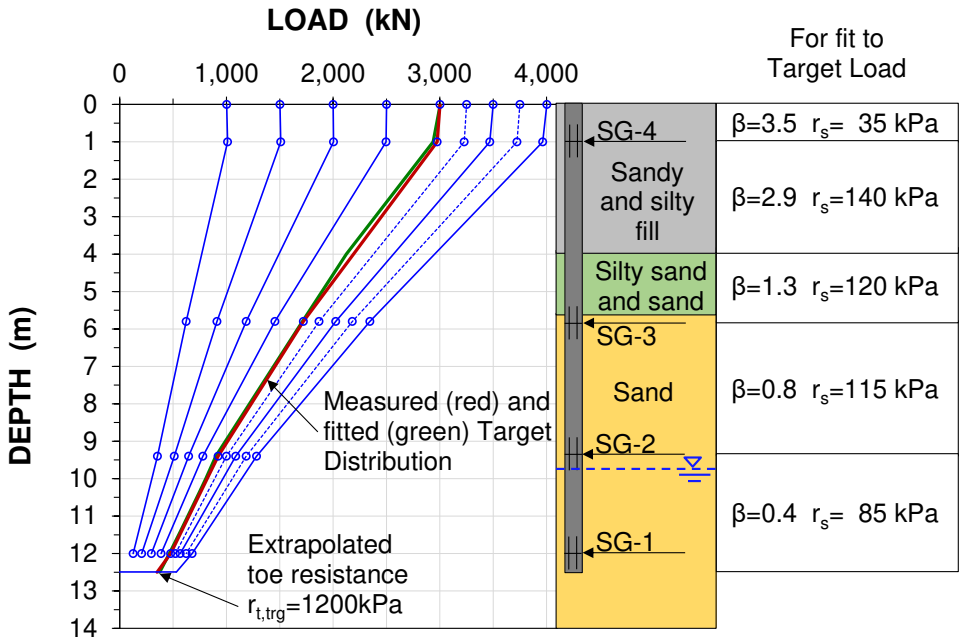

Figure 9. Measured and fitted load distributions.

Residual Force and Beta-Coefficients

The measured unit shaft resistance for the 3,000 kN Target Load, corresponded to a ß-coefficient of 3.5 at the ground surface reducing to about 0.4 at the pile toe level. Unrealistically, the unit shaft resistance back-calculated in the loose sandy and silty fill above 4 m depth was larger than that developed in the dense sand below. This is an indication that the pile was subjected to residual force, i.e., presence of axial force locked in the pile before starting the test (Mascarucci 2013, Fellenius 2015; 2020).

The residual force distribution is built up of negative direction shaft shear in the upper portion of the pile changing to positive direction along some transition length. The associated movement must be small and, presumably, about the movement necessary to build up the Target resistance. In the absence of actual measurements of the distribution of axial force in the pile before the start of the static loading test, the distribution has to be estimated from the distributions induced during the test, as follows. Applying the method of Fellenius et al., (2000), we have assumed that (1) down to SG-3 (≈6.0 m depth), the back-calculated unit shaft resistance comprised of an equal part negative skin friction and positive shaft resistance, (2) between

SG-3 and SG-2, the negative skin friction would start reducing, and (3) at SG-2, the shaft shear due to residual force act in positive direction. Moreover, because of the uniformity of the soil below 6 m depth, the beta coefficient (ratio of the "true" unit shaft resistance to the effective overburden stress) could be assumed about constant with depth below SG-3 to the pile toe level. These assumptions resulted in the "true" distribution of axial force for the Target Load shown in Figure 10. The distribution adjusted for residual force is the green curve marked "Target Distribution w/o Residual Force". Subtracting the back-calculated distribution resulted in the red curve marked "Residual Force". After the correction for residual force, the evaluated unit shaft resistance showed to be more realistic, i.e., gradually increasing with depth, with a ß-coefficient constant and equal to 0.6.

If the unit negative skin friction along the upper length would have been smaller than assumed, the "true" beta-coeffieicnt in the lower portion of the pile would still be reducing with depth, still indicating presence of residual force. If assumed larger, this would have resulted in a larger "true" positive unit shaft resistance above the pile toe as well as a larger and probably overestimated residual toe force.

After adjustment for residual force, the toe resistance would be about 970 kN (mobilized for the Target Load and the 5 mm Target Movement), as opposed to 370 kN, i.e., the residual toe force would be about 600 kN and the "true" toe stress about 3,100 kPa as opposed to 1,200 kPa. Considering the residual toe force, the toe resistance mobilized for the maximum load and the 13 mm toe-movement was about 1,100 kN as opposed to 530 kN, i.e., the "true" toe stress was about 3,500 kPa.

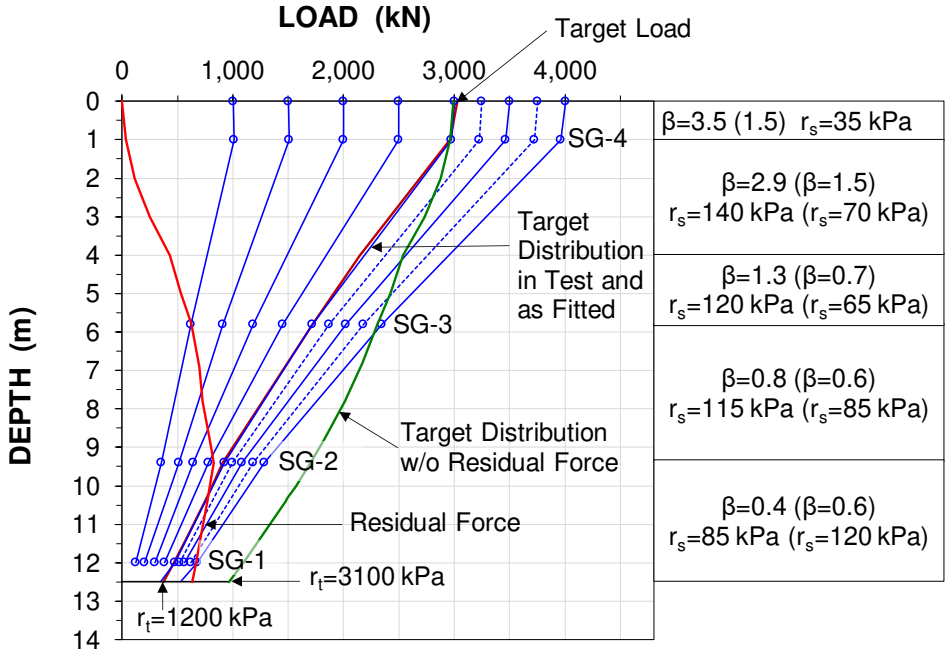

Figure 10. Back-calculated load distributions and distribution for the Target Load with and without residual force.

t-z and q-z Functions

The test records show the measured load at the pile head and include the strain-determined force at the gage levels in respect to the movement measured at the pile head. The next step in the analysis of the test records was to calculate and fit load-movement curves to the measured pile-head curve and the strain-determined curve using t-z functions for the shaft response and a q-z function for the pile toe response (Fellenius 2020). Any t-z/q-z function can be made to intersect a specific load-movement point on a curve. Those points are, of course, the specific targets for the fit to the measured loads. The process comprises choosing a suitable function, which intersects the target. Then, by adjusting the function coefficient, the curve should fit the data points before and beyond the Target Value. The curve-fitting analysis was performed using the UniPile5 software and proceeded by first fitting simulated t-z and q-z functions to the load-movement curve for the SG-1 level, varying the input to the portion between SG-1 and the pile toe until a fit was achieved. Next, the procedure was repeated for 1.0 m long pile elements between SG-2 and SG-1, fitting the calculations to the load at SG-2 and measured pile-head movement.

The input for the first fit was kept intact. Afterwards, the analysis was conducted for SG-3 to SG-2, SG-4 to SG-3, and finally, for the pile head.

Of the several t-z/q-z functions available, ranging from strain-softening response through strain-hardening response, the process showed that only the strain-hardening function, called the "Gwizdala" function (or "Ratio" or "Power" function), could be used to fit the test records (Gwizdała 1996). The function is defined by the following equation:

$$Q_n = Q_{trg}\left(\frac{\delta_n}{\delta_{trg}}\right)^{\theta} \tag{2}$$

where:
Q_n = applied load
Q_{trg} = Target Load (or unit shaft resistance)
δ_n = movement mobilized at Q_n
δ_{trg} = movement mobilized at Q_{trg}
θ = function coefficient

Only two slightly different t-z function coefficients, θ, were needed. Figure 11a shows the measured load-movement curves (solid lines) together with the fitted curves (dashed lines). The latter are extrapolated to twice the actual movements. Figure 11b shows the t-z and q-z curves and the function coefficients that gave the fits.

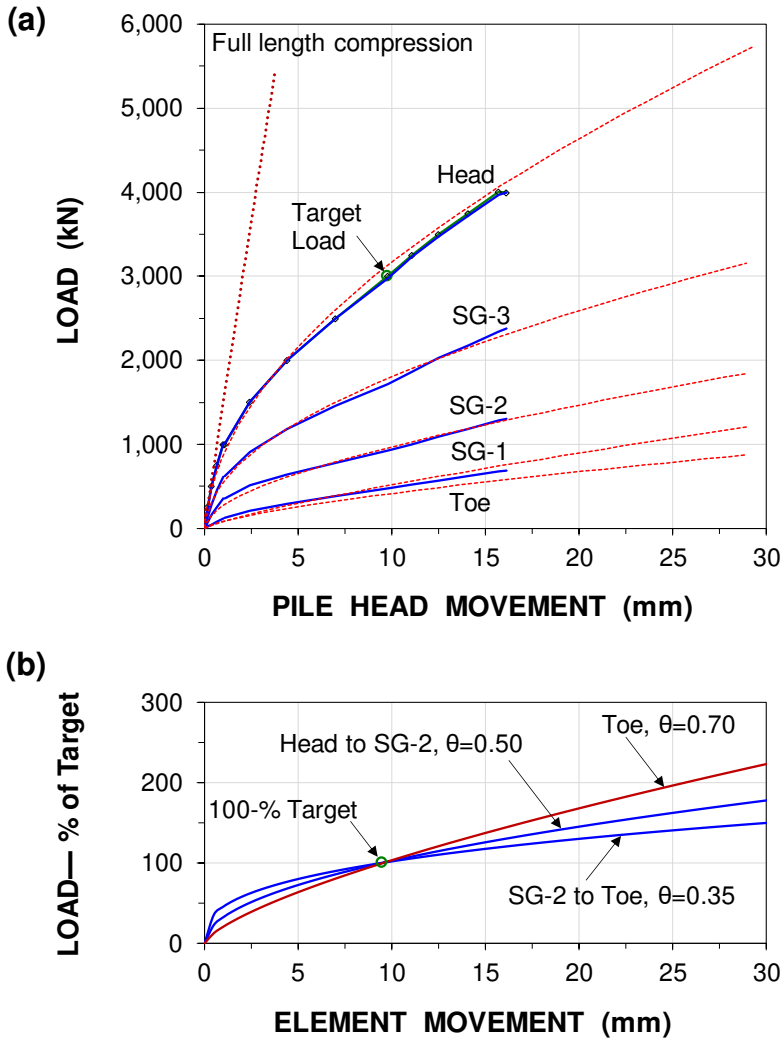

Figure 11. (a) Measured and fitted load-movement curves and (b) the associated t-z/q-z curves.

CONCLUSIONS

The analysis of the strain-gage records showed that the unloading-reloading of the pile at the 1,000 kN load made the stiffness (EA) evaluated per the direct secant method less precise. By correlation to the results of the tangent method, the pile stiffness was determined according to the equation (1) and applied to the strain records to calculate the axial loads in the pile at the gage levels.

The load distribution evaluated for the 3,000 kN Target Load, for which the pile-head movement was 9.8 mm and pile-toe movement was 7.8 mm, showed that about 370 kN reached the pile toe and the unit shaft resistance was largest at shallow depth and reduced significantly with depth. The beta-coefficients for the resistance mobilized by the Target Load were about 3.5 near the ground surface and 0.4 at the pile toe.

The initial back-calculation of the measured strains assumed that the pile was not affected by residual force. However, the evaluated distributions of shaft resistance indicated that residual force was indeed present in the test pile at the start of the test. The most likely distribution of residual force was determined and showed a more consistent mobilization of the pile shaft resistance as well as a 600 kN residual toe force. When adjusted for residual force, the toe resistance mobilized for the maximum load and 13 mm toe-movement was about 1,000 kN as opposed to 530 kN, i.e., the "true" toe stress was about 3,500 kPa. The results show that disregarding the residual force can result in significant error in the evaluation of shaft and toe resistances.

The fit to the measured load-movement curves showed that simulating the response with t-z and q-z functions per the Gwizdala method gave good fits for function coefficients, θ, of 0.70 for the pile toe response, and 0.35 and 0.50 for the length below SG-2 (9.4 m depth) and the length above SG-2, respectively. These coefficients indicated that the soil is strain-hardening and that no ultimate resistance will develop even at movements somewhat larger than the 16 mm maximum imposed in the test.

The results show that the test pile shaft resistance is well within the range of that observed in driven piles and that already the toe resistance mobilized at the 13 mm maximum toe movement was several times larger than the 1,000 kPa limit inidicated in the Danish Annex to the Eurocode. We believe that similar tests on further projects will show that the current Annex is overly restrictive in regard to CFA piles.

ACKNOWLEDGMENTS

The authors would like to thank cp test a/s, Per Aarsleff A/S, Centrum Pæle A/S, DMT Gründungstechnik, GmbH, and Innovation Fund Denmark for providing funding for this study and Per Aarsleff A/S for providing data and for installing the instrumented test pile.

REFERENCES

Aamann-Svale, R., and Møller, O. (2017). *Midtbyens Gymnasium, Viborg. Statisk prøvebelasting*, Aarsleff, Viby J.

Eslami, A. (1996). *Bearing capacity of piles from cone penetrometer test data*, Ph. D. Thesis, University of Ottawa, Department of Civil Engineering.

Fellenius, B.H. (1989). "Tangent modulus of piles determined from strain data." *1989 Foundation Congress by F.H. Kulhawy*, ASCE, 1, 500-510.

Fellenius, B.H. (2012). "Critical assessment of pile modulus determination methods. Discussion." *Canadian Geotechnical Journal*, 49(5), 614-621.

Fellenius, B.H. (2015). "Static tests on instrumented piles affected by residual load." *Journal of the Deep Foundation Institute*, 9(1), 11-20.

Fellenius, B.H. (2020). "Basics of foundation design – a textbook." Electronic Edition, <http://www.fellenius.net/papers/401%20The%20Red%20Book,%20Basics%20of%20Foundation%20Design%202020.pdf>.

Fellenius, B.H., Brusey, W.G., and Pepe, F. (2000). "Soil set-up, variable concrete modulus, and residual load for tapered instrumented piles in sand." *ASCE Specialty Conference on Performance Confirmation of Constructed Geotechnical Facilities*, University of Massachusetts, Amherst, 98-114.

Fellenius, B.H., and Nguyen, B.N. (2019). "Common mistakes in static loading-test procedures and result analyses." *Geotechnical Engineering Journal of the SEAGS & AGSSEA*, 50(3), 20-31.

GEO (2016). *Viborg Banegårds Alle. Gymnasie i 6 etager uden kælder. Geoteknisk og miljøteknisk undersøgelse*, Geo, Brabrand.

Goudreault, P.A., and Fellenius, B.H. (2014). "UniPile Version 5, User and Examples Manual." *UniSoft Geotechnical Solutions Ltd.*, <https://www.fellenius.net/papers/343%20UniPile%20User%20and%20Examples%20Manual.pdf>.

Gwizdała, K. (1984). *Large diameter bored piles in non-cohesive soils*, Swedish Geotechnical Institute. Report no. 26. Linköping.

Gwizdała, K. (1996). *The analysis of pile settlement employing load-transfer functions (in Polish)*, Zeszyty Naukowe Politechniki Gdańskiej, Nr 532, Budownictwo Wodne, nr 41, Gdańsk.

Kania, J.G., and Sørensen, K.K. (2018). "A static pile load test on a bored pile instrumented with distributed fibre optic sensors." *10th International Symposium on Field Measurements in Geomechanics*, Rio de Janerio, Brazil.

Knudsen, J., Sørensen, K.K., Steenfelt, T.J.S., and Trankjær, H. (2019). "Design of bored piles in Denmark–a historical perspective." *XVII European Conference on Soil Mechanics and Geotechnical Engineering*, Reykjavik, Iceland.

Mascarucci, Y., Mandolini, A., and Miliziano, S. (2013). "Effects of residual stresses on shaft friction of bored cast in situ piles in sand." *Journal of Geo-Engineering Sciences*, 1(1), 37-51.

Nguyen, M.H., and Fellenius, B.H. (2013). "Large diameter long bored piles in the Mekong delta." *International Journal of Geoengineering Case Histories*, 2(3) 196-207.

Platzek, P., and Gerressen, F.-W. (2010). "Overview of the state of the art of double rotary drilling methods." *DFI and EFFC 11th International Conference – Geotechnical Challenges in Urban Regeneration,* London.

Touma, F.T., and Reese, L.C. (1972). *The Behavior of Axially Loaded Drilled Shafts in Sand*, Texas Highway Department, Research Report 176-1, Austin.

The open access Mission of the International Journal of Geoengineering Case Histories is made possible by the support of the following organizations:

Access the content of the ISSMGE International Journal of Geoengineering Case Histories at:
https://www.geocasehistoriesjournal.org